fishes

MDPI

Article

Comparative Metabolomic Analysis Reveals the Impact of the Photoperiod on the Hepatopancreas of Chinese Grass Shrimp (*Palaemonetes sinensis*)

Duojia Qu, Chunyan Fu, Muyu Han and Yingdong Li *

College of Animal Science and Veterinary Medicine, Shenyang Agricultural University, Dongling Road 120, Shenyang 110866, China

* Correspondence: liyingdong@syau.edu.cn

Abstract: The photoperiod is a key environmental factor that in crustaceans influences development, feeding, and metabolism. In this study, liquid chromatography-tandem mass spectrometry was used to examine metabolic changes in *Palaemonetes sinensis* under different photoperiods. Our results showed that key metabolic pathways, such as linoleic acid metabolism, axon regeneration, pyrimidine metabolism, and cortisol synthesis, were significantly altered under both constant light (24L:0D) and constant darkness (0L:24D) compared with natural light conditions. The photoperiod notably affected the digestive and metabolic functions of *P. sinensis*. Most metabolic pathways were downregulated under full darkness and full light conditions, suggesting that inhibition of metabolism is a potential adaptive response. Furthermore, enzyme assays revealed significant variations in trypsin, lipase, and amylase activity across different photoperiods, highlighting the profound impact of light conditions on digestive functions. These findings suggest that extreme light conditions may negatively impact the metabolic and digestive functions of *P. sinensis*. This study provides new insights into the adaptive mechanisms of *P. sinensis* in response to photoperiod changes and offers valuable information for optimizing aquaculture practices to enhance the health and growth performance of this crustacean.

Keywords: photoperiod; metabolomics; hepatopancreas; *Palaemonetes sinensis*

Key Contribution: In this study, the metabolic effects of different photoperiods on *P. sinensis* were studied, and the effects of photoperiods on immune and digestive systems were emphasized.

Citation: Qu, D.; Fu, C.; Han, M.; Li, Y. Comparative Metabolomic Analysis Reveals the Impact of the Photoperiod on the Hepatopancreas of Chinese Grass Shrimp (*Palaemonetes sinensis*). *Fishes* **2024**, *9*, 444. https://doi.org/10.3390/fishes9110444

Academic Editors: Weijie Mu and Eric Hallerman

Received: 29 August 2024
Revised: 22 October 2024
Accepted: 29 October 2024
Published: 31 October 2024

1. Introduction

In aquatic ecosystems, the light environment is an important ecological factor, which predominantly refers to light intensity, the photoperiod, and light color (spectral component), and has a profound impact on various physiological processes and the feeding behaviors of aquatic animals [1]. In crustaceans, the photoperiod can affect early growth, survival, metabolism, and the immune system; it regulates the secretion and synthesis of biomolecules and affects biorhythms that are crucial for physiological health [2–4]. Under a photoperiod of 18 h light, juvenile *Cherax quadricarinatus* exhibit high survival rates, improved growth performance, pronounced resistance to oxidative stress, and increased immune defense ability [5]. Continuous lighting and darkness are frequently used to examine the effect of the photoperiod. For example, mud crabs raised in a continuously dark environment increase the triglyceride and total cholesterol content by promoting fat production and fatty acid absorption and inhibiting fat decomposition, thereby affecting the survival and growth performance [6]. In abalone eaters, the proportion and food intake under light conditions were significantly lower than those in darkness, regardless of the light and dark periods [7].

Palaemonetes sinensis, a freshwater shrimp species, is widely distributed in China and Japan [8,9]. This shrimp has been a part of the Chinese diet for centuries and often com-

mands higher market prices than penaeid shrimp [10,11]. In addition, because of their attractive appearance, live *P. sinensis* are popular in the aquarium trade and are frequently used as bait for sports fishing, particularly in Japan [12]. Its growth and reproduction are significantly influenced by the light cycle [13], and in recent years the aquaculture of *P. sinensis* in China, particularly in rice fields and ponds, has expanded significantly because of a pronounced decline in wild populations [10,14,15]. As farming efforts intensify to meet the demand, managing environmental factors has become increasingly important for sustainable production. Therefore, understanding the role of the photoperiod in the life cycle of this shrimp is crucial for optimizing both commercial breeding and conservation efforts.

Metabolomics characterizes small organic molecules and reveals the biochemical and physiological states of organisms under various environmental conditions [16]. Various studies have examined the effects of light on the metabolic characteristics of aquatic organisms. For example, Hilly et al. [17] investigated how artificial light at night affected metabolism in the brain, liver, and muscle tissues of the blue-green chromis (*Chromis viridis*), revealing complex tissue-specific metabolic changes that may reduce the fitness of coastal fish. Altered circadian rhythms in *Eriocheir sinensis* lead to differential hepatopancreatic metabolites enriched in circadian rhythm-related pathways, which affect digestive and immune functions [18]. However, metabolomic studies on photoenvironmental factors, especially the photoperiod, are limited with regard to *P. sinensis*, highlighting a research gap in this field. To address this gap, we employed liquid chromatography-tandem mass spectrometry (LC/MS/MS) because of its high sensitivity and selectivity, and because it is particularly well suited to nonvolatile compounds, making it an ideal tool for profiling metabolic changes in response to environmental factors, such as the photoperiod.

To address the research gap regarding the effects of photoperiod on *P. sinensis*, we analyzed the metabolic profiles of the hepatopancreas under various light conditions: full light (24 h light, 0 h darkness [24L:0D]), total darkness (0L:24D), and natural light (10L:14D). By examining these metabolic changes, our study aimed to uncover how photoperiod influences key physiological processes, such as digestion, metabolism, and immune function. Specifically, we sought to identify the respective metabolic pathways.

2. Materials and Methods

2.1. Ethics Statement

This study did not include endangered or protected species. In China, no permits are required to catch grass shrimps. Experiments were performed in accordance with the guidelines on the care and use of animals for scientific purposes set by the Animal Ethics Committee of Shenyang Agricultural University. All efforts were made to minimize animal suffering [11].

2.2. Experimental Design

Three light environments were designed for this experiment: natural light (C1, 10L:14D), full light (C2, 24L:0D; full spectrum, water surface light intensity 1000 lx $\pm$ 50 lx), and total darkness (C3, 0L:24D). The natural light group served as a control. Three replicates of each group were used, and each replicate contained 210 randomly assigned shrimp (average weight 0.725 $\pm$ 0.2 g).

The experiment was conducted in turnover tanks (60 $\times$ 40 $\times$ 23 cm, dark gray) with a continuous oxygen supply and a water volume of 28 L. The water was changed every 2 days, replacing one-third of the volume each time, and the natural temperature was maintained at 12 $\pm$ 1 °C (October). The shrimp were fed water fleas at 2% of their body weight once daily, with adjustments based on the feeding conditions. The remaining bait and feces were removed within 2 h, and the tanks were maintained under consistent feeding methods and environmental conditions.

2.3. Sample Collection

The experiment lasted for 4 weeks. At the end of the experiment, the final body weights were measured, and the number of shrimp deaths was recorded. Feeding was stopped 24 h before sampling to prevent the feeding and digestion processes from affecting the hepatopancreas metabolism [19,20]. The shrimps were anesthetized with ice and killed. Hepatopancreatic tissue samples were collected using sterile scalpels and tweezers. Samples from each replicate were placed in 2 mL RNA-free tubes and stored at −80 °C.

Weight gain and survival of the shrimp were calculated based on the formulae:

$$Weight\ gain(\%) = \frac{final\ weight - initial\ weight}{initial\ weight} \times 100\%, \quad (1)$$

$$Survival\ rate(\%) = \frac{final\ shrimp\ number - initial\ shrimp\ number}{initial\ shrimp\ number} \times 100\% \quad (2)$$

2.4. Enzyme Activity Assay

Commercial kits for trypsin, lipase (LPS), and amylase (AMS) obtained from Nanjing Jiancheng Bioengineering Institute (Nanjing, China) were used to measure their respective activity levels. For enzymatic activity, hepatopancreatic tissue samples were weighed and homogenized (1:9 w/v) in a cold (4 °C) normal saline.

Activity of amylase: One milligram of protein in the tissue was allowed to interact with the substrate at 37 °C for 30 min, and hydrolyzed 10 mg of starch was defined as 1 unit of amylase activity of lipase: under the condition of 37 °C, each gram of hiprotein reacted with the substrate in this reaction system for 1 min, and each consumption of 1 μmol of substrate was considered one unit of enzyme activity. Activity of trypsin: At pH 8.0 and 37 °C, the absorbance change of trypsin per milligram of protein by 0.003 per minute was considered a unit of enzyme activity.

2.5. Hepatopancreas Metabolomic Analysis

The hepatopancreas samples were thawed at 4 °C and vortexed for 1 min. An appropriate amount of each sample was transferred into a 2 mL centrifuge tube, followed by the addition of 400 μL methanol and vortexing for 1 min. The samples were centrifuged at 12,000 rpm and 4 °C for 10 min. The supernatant was transferred to a new 2 mL centrifuge tube, concentrated, and dried. Finally, 150 μL 2-chloro-L-phenylalanine (4 ppm) in 80% methanol was added to redissolve the samples. The supernatant was filtered through a 0.22 μm membrane and transferred to vials for LC-MS detection.

LC analysis was performed on a Vanquish UHPLC System (Thermo Fisher Scientific, Waltham, MA, USA) using an ACQUITY UPLC® HSS T3 column (2.1 × 100 mm, 1.8 μm) (Waters, Milford, MA, USA) at 40 °C. The flow rate was 0.3 mL/min, with an injection volume of 2 μL.

For LC-ESI (+)-MS analysis, the mobile phases used were 0.1% formic acid in acetonitrile (B2) and 0.1% formic acid in water (A2). The gradient was: 0–1 min, 8% B2; 1–8 min, 8–98% B2; 8–10 min, 98% B2; 10–10.1 min, 98–8% B2; 10.1–12 min, 8% B2. For LC-ESI (−)-MS analysis, the mobile phases were acetonitrile (B3) and 5 mM ammonium formate (A3). The gradient was: 0–1 min, 8% B3; 1–8 min, 8–98% B3; 8–10 min, 98% B3; 10–10.1 min, 98–8% B3; 10.1–12 min, 8% B3.

Mass spectrometric detection was performed on an Orbitrap Exploris 120 (Thermo Fisher Scientific) with an ESI ion source in full MS-ddMS2 mode. The parameters were: sheath gas pressure, 40 arb; auxiliary gas flow, 10 arb; spray voltage, 3.50 kV for ESI(+) and −2.50 kV for ESI(−); capillary temperature, 325 °C; MS1 range, m/z 100–1000; MS1 resolving power, 60,000 FWHM; number of data-dependent scans per cycle, four; MS/MS resolving power, 15,000.

2.6. Analysis of Differential Metabolites

An R package Ropls [21] was used to perform principal component analysis, partial least squares discriminant analysis (PLS-DA), and orthogonal partial least squares discriminant analysis (OPLS-DA) to reduce the dimensionality of the sample data. The score, loading, and S plots illustrate the differences in metabolic composition among the samples. Overfitting was assessed using permutation testing. R2X and R2Y indicate the explained variances for the X and Y matrices, respectively, whereas Q2 reflects the predictive capability of the model. Higher values approaching 1 indicate a better model fit and accurate classification. Metabolites with $p < 0.05$ and variable importance of projection (VIP) > 1 were considered statistically significant.

Differential metabolite abundances were analyzed using a Pheatmap package (version 1.0.12) to generate heatmaps and trend plots. Venn diagrams and UpSet plots for the differentially expressed substances in the two-group comparisons were created using VennDiagram (version 1.7.3) and UpSetR (version 1.4.0). Correlation analysis was conducted using corrplot (version 4.0.3) and box and violin plots were generated using ggplot2 (version 3.4.1). Machine learning analysis (mlr3verse, version 0.2.7) and receiver operating curve (ROC) plotting (pROC, version 1.18.2) were used to identify key metabolites. Functional analysis involved Kyoto Encyclopedia of Genes and Genomes (KEGG) enrichment using clusterProfiler (version 4.6.0), highlighting significantly enriched pathways, and calculating differential abundance scores to identify critical pathways.

2.7. Statistical Analysis

The original data were converted to mzXML format using ProteoWizard(V 3.0.8789). Peak alignment, retention time correction, and peak area extraction were performed using XCMS software (V3.0). Metabolite identification and data preprocessing were conducted, followed by quality evaluation of the experimental data. Subsequent analyses included univariate and multidimensional statistical analyses, differential metabolite screening, correlation analysis, machine learning, ROC analysis, and KEGG pathway analysis.

3. Results

3.1. Survival and Growth Performance

As shown in (Table 1), the 0L:24D group exhibited the highest survival rate, which was in stark contrast to the lowest survival rate observed in the 10L:14D group. The 10L:14D group showed the highest weight gain, whereas the 24L:0D group showed the lowest weight gain.

Table 1. Effects of different photoperiods on the survival and growth performance of *P. sinensis*.

Items	10L:14D	24L:0D	0L:24D
Survive rate (%)	91.83 ± 3.13	93.43 ± 2.32	96.13 ± 0.45
Weight gain rate (%)	10.93 ± 0.02	6.08 ± 0.02	8.80 ± 0.03

3.2. Quality Control and Data Checking

Pearson's correlation analysis was conducted on the QC samples to assess the similarity of expression patterns. A correlation coefficient close to 1 indicates a high similarity, with values greater than 0.9 generally signifying good correlation. The results demonstrated that the correlation coefficients between the QC samples were consistently above 0.9, confirming high experimental repeatability (Figure 1).

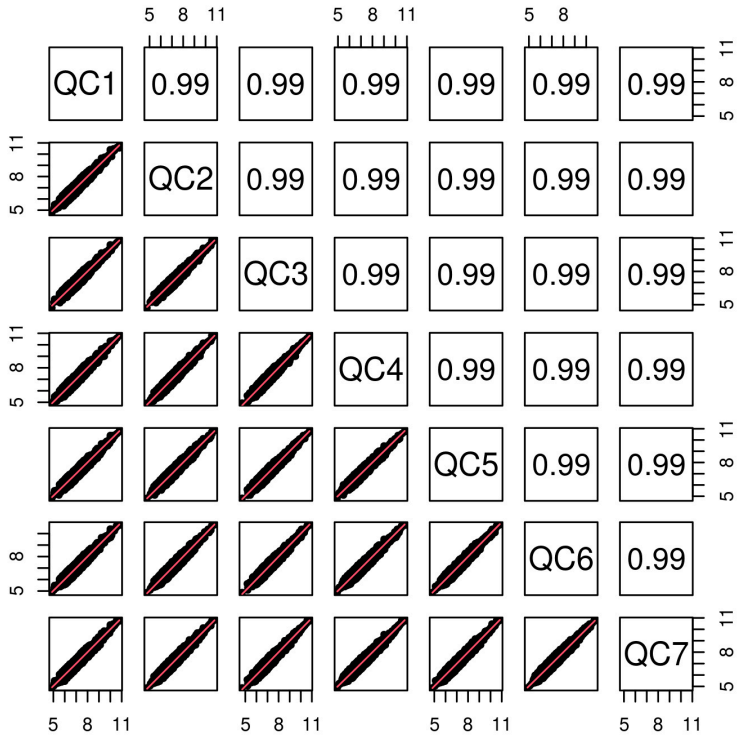

Figure 1. Horizontal and vertical coordinates in the figure represent QC samples. The points in each cell represent the ion peak (metabolite) extracted from QC samples, and the horizontal and vertical coordinates represent the pair value of the ion peak signal strength value. The value in the figure is the correlation coefficient value, and the coefficient greater than 0.9 is considered to be highly correlated.

3.3. Enzyme Activity

Figure 2 shows enzyme activity over time under different light−dark cycles. Specifically, trypsin activity was higher in the 10L:14D treatment, whereas no difference was observed between the 24L:0D and 0L:24D treatments. LPS activity was higher in the 0L:24D treatment group, whereas no difference was observed between the 24L:0D and 10L:14D treatments. AMS activity did not differ among the treatments. These findings indicate that varying photoperiods significantly affect the enzyme activities of these substances.

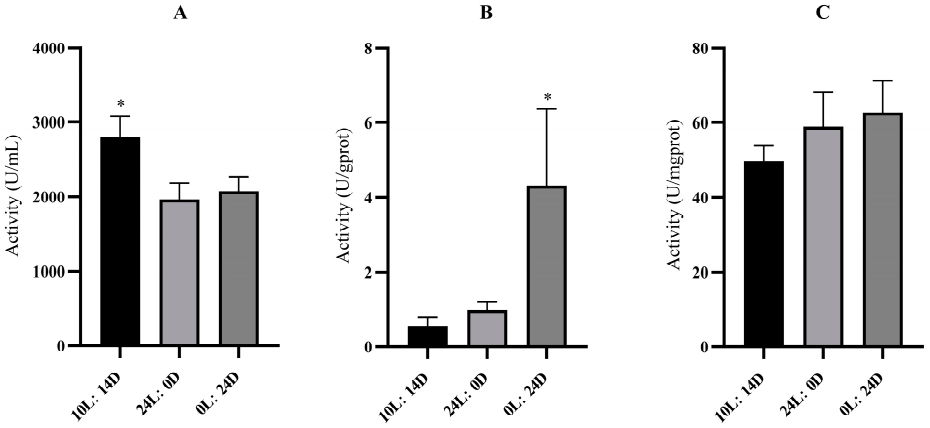

Figure 2. Enzyme activity profiles of Trypsin (**A**), LPS (**B**), and AMS (**C**) of hepatopancreas tissue samples in *Palaemonetes sinensis* under different photoperiod conditions. Data are presented as mean ± standard deviation (n = 3). Points of different colors represent metabolites identified in different photoperiods. Asterisks indicate significant differences.

3.4. Metabolite Identification and Comparison

The results shown in Figure 3 reveal a clear separation between the 10L:14D, 24L:0D, and 0L:24D conditions in both positive and negative ion modes. This separation indicated that changes in the photoperiod significantly affected the metabolic status of P. sinensis.

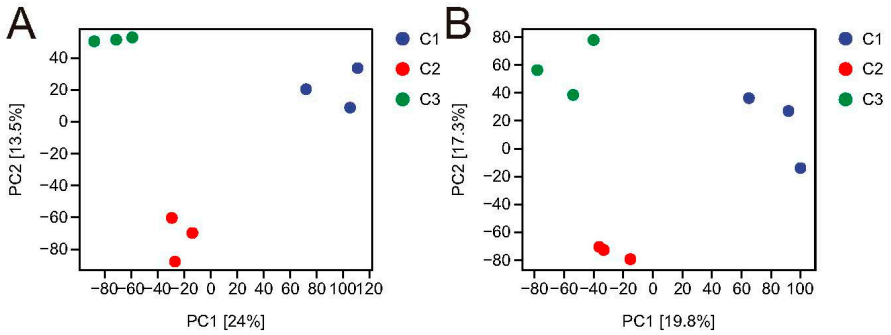

Figure 3. The multivariate data analysis. The PLS-DA score plots of hepatopancreatic samples in positive mode (**A**) and negative mode (**B**). Points of different colors represent metabolites identified at different photoperiods.

3.5. Identification of Metabolites with Significant Differences

A total of 305 differentially expressed metabolites were identified, with fatty acyls accounting for 39.73% of them. Carboxylic acids and derivatives accounted for 19.18% of the differential metabolites, whereas organo−oxygen compounds represented 6.85% (Figure S1).

3.6. Comparison of Hepatopancreatic Metabolites

Differential metabolites were identified based on VIP ≥ 1 and $p \leq 0.05$. Under full light conditions, 20 differential metabolites were identified compared to natural light conditions, with 2 metabolites upregulated and 18 downregulated (Table 2). These metabolites were primarily associated with indoles and their derivatives, fatty acyl groups, and related families. Under full darkness, 39 differential metabolites were identified, of which 11 were upregulated and 28 were downregulated (Table 3). These metabolites were mainly concentrated in indole and its derivatives, fatty acyl groups, and carboxylic acids. Most of the differentially expressed metabolites were linked to immunity and energy metabolism.

Table 2. Hepatopancreatic differential metabolites among 10L:14D and 24L:0D.

Regulation	Name	VIP	Fold Change	*p*-Value	FDR
Up	Anabasine	1.907297316	3.158097785	1.74×10^{-5}	0.318782
	Methoprene	1.684382823	2.780965383	0.0258962	0.656741
Down	3-Hydroxymethylglutaric acid	1.905099882	0.190579202	0.0009552	0.403403
	Guanosine	1.911404573	0.466353051	0.00236	0.654583
	Maltol	1.837813673	0.119762921	0.0025269	0.46636
	Agmatine	1.832581464	0.212675525	0.0035182	0.488711
	Palmitoyl-L-carnitine	1.871665251	0.421684127	0.0037924	0.488711
	Indole	1.809790956	0.862476991	0.0069588	0.535137
	L-Tryptophan	1.783906192	0.866652658	0.0086536	0.553457
	3-Dehydroshikimate	1.730013181	0.853776833	0.015607	0.606582
	12-Keto-leukotriene B4	1.720753783	0.58867918	0.0208922	0.790759
	3-Methylindole	1.662382191	0.88113951	0.0253116	0.65533
	Taurocholic acid	1.69563276	0.414046236	0.025464	0.656555
	4-Acetylbutyrate	1.762004096	0.862065771	0.0287383	0.663664
	1,5-Naphthalenediamine	1.636454482	0.896950592	0.0308542	0.670219
	Cytidine	1.705254513	0.424843618	0.0318796	0.672933
	Uridine	1.701526212	0.435161805	0.0343067	0.790759

Table 2. *Cont.*

Regulation	Name	VIP	Fold Change	*p*-Value	FDR
Down	8-Amino-7-oxononanoate	1.592304996	0.68752891	0.0432281	0.68288
	Kinetin	1.641848437	0.66737036	0.044375	0.68288
	N-Alpha-acetyllysine	1.58166688	0.876164025	0.0481752	0.686258

Table 3. Hepatopancreatic differential metabolites among 10L:14D and 0L:24D.

Regulation	Name	VIP	Fold Change	*p*-Value	FDR
Up	12,13-DHOME	1.848892946	7.944503725	0.0025492	0.435487
	Vanillylmandelic acid	1.698582067	2.287584995	0.0146389	0.572589
	1-Hexadecanol	1.608151478	2.041461624	0.0173203	0.304102
	Deoxyuridine	1.587256606	1.272344109	0.0219119	0.322259
	PC(18_3(6Z,9Z,12Z)_18_3(6Z,9Z,12Z))	1.624879576	9.744630256	0.0231141	0.329669
	Glutathionylspermidine	1.475731058	4.137433822	0.0314225	0.350268
	Porphobilinogen	1.466742525	2.877259275	0.0369976	0.364777
	Gamma-Linolenic acid	1.65502262	1.365807338	0.0378202	0.612128
	Alpha-dimorphecolic acid	1.618926287	2.597285846	0.040452	0.614582
	7,8-Diaminononanoate	1.507837379	1.273066329	0.0419005	0.374433
	8,11,14-Eicosatrienoic acid	1.513521616	2.351772099	0.0429527	0.378504
Down	(R)-4-Hydroxymandelate	1.71739743	0.776230178	0.0001679	0.163141
	N-Methyltryptamine	1.834687656	0.302541618	0.0018306	0.398592
	Guanosine 3′-phosphate	1.661328012	0.55848625	0.0029291	0.22165
	Guanosine	1.820377684	0.368505666	0.0039691	0.483225
	Indole	1.640341233	0.848668536	0.0064791	0.246949
	Taurine	1.592918474	0.715815838	0.0106643	0.27098
	CMP	1.563437429	0.571401423	0.0115314	0.276959
	4-Acetylbutyrate	1.588548367	0.842573158	0.0121322	0.281471
	3-Dehydroshikimate	1.560734708	0.860089133	0.0125116	0.284814
	1,5-Naphthalenediamine	1.598978464	0.869860663	0.0132279	0.287593
	3-Methylindole	1.593774137	0.865101666	0.0145031	0.291362
	4-Guanidinobutanoic acid	1.651596962	0.160116061	0.0150216	0.292051
	8-Amino-7-oxononanoate	1.553996072	0.59167106	0.0151476	0.292051
	Cytidine	1.659082161	0.251674321	0.0181636	0.309742
	L-Tryptophan	1.526508918	0.886507002	0.0186632	0.311918
	Guanidoacetic acid	1.520163573	0.829851625	0.0199308	0.315627
	Palmitoyl-L-carnitine	1.569867597	0.310984095	0.0305007	0.348488
	Uridine	1.665952542	0.408655048	0.0342888	0.607128
	Glycitein	1.576053112	0.317608942	0.034728	0.359354
	Cortexolone	1.521167154	0.533997038	0.0353217	0.360789
	Propionylcarnitine	1.532435504	0.612049756	0.0389239	0.367213
	Pyrrolidonecarboxylic acid	1.58033653	0.255350103	0.0446104	0.384618
	D-Galactose	1.68348797	0.455843304	0.045287	0.619777
	epsilon-(gamma-L-Glutamyl)-L-lysine	1.418573297	0.621361739	0.0462443	0.388083
	Cyclic AMP	1.430922335	0.625015239	0.046507	0.389122
	Kinetin	1.560722322	0.783293537	0.0472655	0.390247
	Creatinine	1.404212767	0.71705939	0.0473558	0.390353
	Saccharopine	1.484150092	0.839835089	0.048923	0.393707

Notably, L-tryptophan and 3-methylindole were downregulated under both full light and full darkness conditions compared to natural light. Tryptophan is an amino acid with an indole structure that can be converted to 3-methylindole, which is associated with immune regulation. Gamma-linolenic acid and 8, 11, 14-eicosatrienoic acid were upregulated in the linoleic acid metabolism pathway, and linoleic acid metabolism was associated with an immune response and lipid metabolism. Both full light and dark conditions affect the immune system of *P. sinensis*.

3.7. KEGG Pathway Analysis of Key Metabolic Pathways

Functional enrichment analysis of the identified differential metabolites revealed that the metabolism of *P. sinensis* was influenced by the photoperiod (Figures S2 and S3). Key metabolic pathways affected include "metabolism" and "organismic systems". Enrichment was assessed using the Rich factor, false discovery rate (FDR) values, and number of metabolites in each pathway. The Rich factor represents the ratio of differential metabolites in a pathway to the total number annotated, with a higher Rich factor indicating greater enrichment. An FDR closer to zero signifies a more significant enrichment.

The top 20 KEGG pathways with the smallest FDR values, indicating the most significant enrichment, are shown. Each point represents a metabolic pathway, with color coding corresponding to FDR values and the dot size representing the number of metabolic molecules in the pathway.

Using FDR < 1 and $p < 0.05$ as criteria, the following pathways were significantly enriched between the natural light control group (10L:14D) and the full light treatment group (24L:0D): phenylalanine, tyrosine, and tryptophan biosynthesis; tryptophan metabolism; ABC transporters; protein digestion and absorption; pyrimidine metabolism; axon regeneration; and cholesterol metabolism (Table 4). For comparisons between the natural light control group (10L:14D) and the total darkness treatment group (0L:24D), the significantly enriched pathways included linoleic acid metabolism; axon regeneration; pyrimidine metabolism; phenylalanine, tyrosine, and tryptophan biosynthesis; tryptophan metabolism; ABC transporters; cortisol synthesis and secretion; and biotin metabolism (Table 5).

Table 4. KEGG pathway analysis 10L:14D vs. 24L:0D.

Pathway	Total	Hits	*p*-Value	FDR	Compounds
Phenylalanine, tyrosine and tryptophan biosynthesis	35	3	0.000138	0.00344	L-Tryptophan; Indole; 3-Dehydroshikimate
Tryptophan metabolism	83	3	0.001774	0.022176	L-Tryptophan; Indole; 3-Methylindole
ABC transporters	138	3	0.007504	0.053808	Uridine; Guanosine; Cytidine
Protein digestion and absorption	47	2	0.008609	0.053808	L-Tryptophan; Indole
Pyrimidine metabolism	64	2	0.015593	0.077965	Uridine; Cytidine
Axon regeneration	7	1	0.021192	0.088298	L-Tryptophan
Cholesterol metabolism	10	1	0.030146	0.107665	Taurocholic acid

Table 5. KEGG pathway analysis 10L:14D vs. 0L:24D.

Pathway	Total	Hits	*p*-Value	FDR	Compounds
Linoleic acid metabolism	28	5	1.51×10^{-6}	0.00014	PC(18_3(6Z,9Z,12Z)_18_3(6Z,9Z,12Z)); 8,11,14-Eicosatrienoic acid; Gamma-Linolenic acid; Alpha-dimorphecolic; 12,13-DHOME
Pyrimidine metabolism	64	4	0.001217	0.037738	CMP; Uridine; Cytidine; Deoxyuridine
ABC transporters	138	5	0.003307	0.045784	Taurine; Uridine; Guanosine; Cytidine; Deoxyuridine
Retrograde endocannabinoid signaling	19	2	0.008641	0.089285	Cyclic AMP; PC(18_3(6Z,9Z,12Z)_18_3(6Z,9Z,12Z))
Biotin metabolism	29	2	0.019579	0.121392	8-Amino-7-oxononanoate; 7,8-Diaminononanoate
PPAR signaling pathway	5	1	0.037033	0.136271	Alpha-dimorphecolic acid
Axon regeneration	7	2	0.001123	0.037738	L-Tryptophan; Cyclic AMP
Phenylalanine, tyrosine and tryptophan biosynthesis	35	3	0.002144	0.045784	L-Tryptophan; Indole; 3-Dehydroshikimate
Tryptophan metabolism	83	4	0.003186	0.045784	L-Tryptophan; Indole; N-Methyltryptamine; 3-Methylindole
Cortisol synthesis and secretion	12	2	0.003446	0.045784	Cyclic AMP; Cortexolone
Hedgehog signaling pathway	1	1	0.007515	0.087365	Cyclic AMP
Arginine and proline metabolism	69	3	0.014438	0.107135	Guanidoacetic acid; Creatinine; 4-Guanidinobutanoic acid
Longevity regulating pathway—multiple species	2	1	0.014976	0.107135	Cyclic AMP
Circadian rhythm	2	1	0.014976	0.107135	Cyclic AMP
Vasopressin-regulated water reabsorption	2	1	0.014976	0.107135	Cyclic AMP
Mineral absorption	29	2	0.019579	0.121392	L-Tryptophan; D-Galactose
Oocyte meiosis	4	1	0.029734	0.136271	Cyclic AMP
Leukocyte transendothelial migration	4	1	0.029734	0.136271	Cyclic AMP
Insulin signaling pathway	4	1	0.029734	0.136271	Cyclic AMP

Table 5. *Cont.*

Pathway	Total	Hits	*p*-Value	FDR	Compounds
Progesterone-mediated oocyte maturation	4	1	0.029734	0.136271	Cyclic AMP
Growth hormone synthesis, secretion and action	4	1	0.029734	0.136271	Cyclic AMP
MAPK signaling pathway	5	1	0.037033	0.136271	Cyclic AMP
Rap1 signaling pathway	5	1	0.037033	0.136271	Cyclic AMP
Chemokine signaling pathway	5	1	0.037033	0.136271	Cyclic AMP
Purine metabolism	101	3	0.039073	0.136271	Guanosine; Cyclic AMP; Guanosine 3′-phosphate
Serotonergic synapse	42	2	0.03909	0.136271	L-Tryptophan; Cyclic AMP
GnRH signaling pathway	6	1	0.044278	0.136271	Cyclic AMP
Melanogenesis	6	1	0.044278	0.136271	Cyclic AMP
Relaxin signaling pathway	6	1	0.044278	0.136271	Cyclic AMP
Protein digestion and absorption	47	2	0.047956	0.136271	L-Tryptophan; Indole
Glycine, serine and threonine metabolism	48	2	0.04981	0.136271	L-Tryptophan; Guanidoacetic acid

3.8. Cluster Analysis

After stratified cluster analysis, we observed clear trends in metabolite clustering patterns between samples, and the results showed significant differences in metabolite content between the control and experimental groups. The treatment groups (24L:0D) and (0L:24D) were compared with the control group (10L:14D), and the clustering correlation was good (Figure 4).

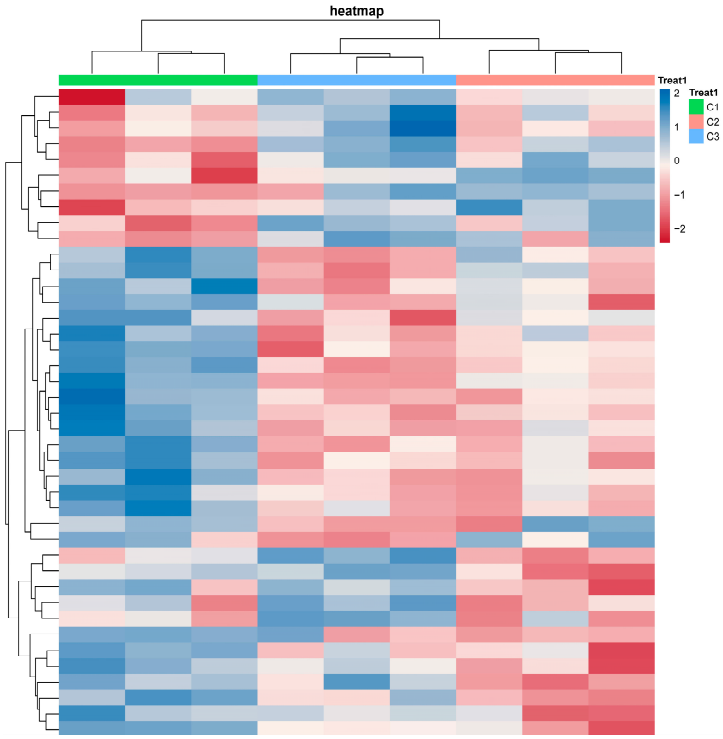

Figure 4. The heatmap of hepatopancreatic samples by cluster analysis. The relative quantitative value of metabolites is displayed by different colors. Columns represent the different photoperiod and rows represent metabolites.

4. Discussion

4.1. Effects on Immune Function

Differential metabolites such as uridine and cytidine, which were enriched in the ABC transporter pathway, were downregulated. This suggests the partial suppression of ABC transporters in the hepatopancreas of *P. sinensis* under full light (24L:0D) and

total darkness (0L:24D). ABC transporters and transmembrane proteins are crucial for transporting various metabolites, including sugars, amino acids, and proteins. They also facilitate the secretion of immune factors and play a role in immune responses [22,23]. Tryptophan, an amino acid with an indole structure, is converted into 3-methylindole, an endogenous AhR ligand that modulates immune functions by activating AhR [24]. This suggests that tryptophan and its metabolites play significant roles in immune regulation.

Additionally, total darkness reduced the cyclic adenosine monophosphate (cAMP) levels in *P. sinensis*. cAMP is a key second messenger involved in various metabolic pathways, including cortisol synthesis and secretion, Hedgehog signaling, and cell differentiation [25]. It also influences axon regeneration in the central nervous system [26]. Both cAMP and cortexolone were co-enriched and downregulated in the cortisol synthesis and secretion pathways. Cortisol mediates stress effects on immune and physiological responses in fish, as it influences food intake regulators and clock gene rhythms, and exhibits circadian variations in stress markers, such as cortisol levels and oxidative stress indicators [27,28]. Thus, the immune system of *P. sinensis* is likely affected by dark environments.

4.2. Effects on the Digestive System

The hepatopancreas is the main digestive organ in crustaceans and plays important roles in nutrient absorption and metabolism, mineral storage, energy storage, and digestive enzyme synthesis [18]. Our study found that tryptophan biosynthesis and metabolic pathways significantly differed between the (10L:14D) and (24L:0D), indicating a notable impact of the photoperiod on digestive function.

Tryptophan is required for protein deposition and for various metabolic functions such as the synthesis of insulin and immune function. In our study, the activity of trypsin, a key digestive enzyme, showed a marked increase under continuous light (24L:0D) conditions, reaching a peak after 24 h. This suggests that prolonged light conditions may enhance protein digestion and nutrient utilization, reflecting an adaptation to a constant light environment. Moreover, the present study found that tryptophan biosynthesis and metabolic pathways differed significantly between 10L:14D and 24L:0D. Photoperiod significantly affects the digestive system in crustaceans. In *Macrobrachium tenellum*, an optimal 14L/10D photoperiod enhances chitinase activity and growth [29], whereas in *Panulirus homarus*, a 12L/12D photoperiod promotes higher activities of digestive and antioxidant enzymes, which are crucial for growth and physiological balance [30].

4.3. Influence on Metabolism and Energy Metabolism

Continuous darkness (0L:24D) affected the biotin metabolism in *P. sinensis*. Biotin, also known as vitamin H, is a member of the vitamin B complex and is readily stored and excreted. Most excess biotin is eliminated through feces and urine, which helps regulate its levels in the body. Biotin plays a crucial role in promoting the metabolism and is essential for maintaining normal physiological activities and the overall health of shrimp [31]. Therefore, biotin metabolism in *P. sinensis* may be closely linked to the metabolic processes.

While no studies have yet demonstrated the effect of the photoperiod on biotin metabolism in crustaceans, extensive research has confirmed that photoperiod influence. Our findings indicate that the downregulation of metabolites such as uridine and cytidine is enriched in the ABC transporter and pyrimidine metabolism pathways, suggesting partial inhibition of these pathways in the hepatopancreas under both full light (24L:0D) and full darkness (0L:24D). ABC transporters, a class of transmembrane proteins, are crucial for the transport of various metabolites across membranes, utilizing energy from ATP hydrolysis to move substrates against concentration gradients [22]. This finding implies a significant relationship between ABC transporters and energy metabolism.

5. Conclusions

In this study, we investigated the effects of different photoperiods on the metabolism of *Palaemonetes sinensis*. These results indicate that variations in the photoperiod can

significantly affect the immune and digestive systems of *P. sinensis*. Compared with natural light conditions, both full light and complete darkness alter the body's immunity, with most metabolic pathways downregulated under full light conditions. This downregulation likely serves as an adaptive mechanism in *P. sinensis*, allowing it to reduce its metabolic activity in response to constant illumination. These findings underscore the importance of understanding the effects of the photoperiod on the health and metabolism of *P. sinensis* and provide a foundation for optimizing aquaculture practices. Future research should focus on exploring specific metabolic pathways influenced by the photoperiod and investigating the long-term effects of different light conditions on growth and reproduction.

Supplementary Materials: The following supporting information can be downloaded at: https://www.mdpi.com/article/10.3390/fishes9110444/s1, Table S1: The metabolomic data. Figure S1: Classification and identification of different metabolites. Each color represents a class of substances, and the percentage represents the percentage of metabolites identified as the substance in the total metabolites. Figure S2: Overview of the significantly enriched KEGG pathways for the significantly different metabolites (SDMs) in the hepatopancreas samples of *Palaemonetes sinensis* comparing the (10L:14D) group to the (24L:0D). Figure S3: Overview of the significantly enriched KEGG pathways for the significantly different metabolites (SDMs) in the hepatopancreas samples of *Palaemonetes sinensis* comparing the (10L:14D) versus the (0L:24D).

Author Contributions: Conceptualization, D.Q. and Y.L.; methodology, D.Q.; software, C.F.; validation, M.H.; formal analysis, C.F.; investigation, D.Q.; resources, Y.L.; data curation, D.Q.; writing—original draft preparation, D.Q.; writing—review and editing, Y.L.; visualization, M.H.; supervision, Y.L.; project administration, Y.L.; funding acquisition, Y.L. All authors have read and agreed to the published version of the manuscript.

Funding: This work was supported by the Dandong Marine and Fisheries Development Service Center "Development and Utilization of Supplementary Live Feed (Small Shrimp) for Indigenous Fish Species in Dandong)" Project. Project number: 2024.

Institutional Review Board Statement: The animal study protocol was approved by the Shenyang Agricultural University Application for Laboratory Animal Welfare and Ethics (protocol code 2023041601 and date of approval 4 October 2023).

Data Availability Statement: The metabolomics data reported in this paper are available via Supplementary Table S1.

Acknowledgments: We thank the Bio JuXing Aquatic Oganism Co. Ltd. for providing the shrimp.

Conflicts of Interest: The authors declare no conflicts of interest.

References

1. Frimmel, F.H. Impact of light on the properties of aquatic natural organic matter. *Environ. Int.* **1998**, *24*, 559–571. [CrossRef]
2. Han, Z.; Li, X.; Xu, W.; She, Q.; Liang, S.; Li, X.; Li, Y. Melatonin concentrations in Chinese mitten crabs *(Eriocheir sinesis*) are affected by artificial photoperiods. *Biol. Rhythm Res.* **2020**, *51*, 362–372. [CrossRef]
3. Zhang, B.; Yu, C.; Xu, Y.; Huang, Z.; Cai, Y.; Li, Y. Hepatopancreas immune response during different photoperiods in the Chinese mitten crab, *Eriocheir sinensis*. *Fish Shellfish Immunol.* **2023**, *132*, 108482. [CrossRef] [PubMed]
4. Zhang, B.; Chai, Y.; Xu, Y.; Huang, Z.; Hu, X.; Li, Y. Impact analysis of photoperiodic disorder on the eyestalk of Chinese mitten crab (*Eriocheir sinensis*) through high-throughput sequencing technology. *Life* **2024**, *14*, 209. [CrossRef]
5. Nie, X.; Huang, C.; Wei, J.; Wang, Y.; Hong, K.; Mu, X.; Liu, C.; Chu, Z.; Zhu, X.; Yu, L. Effects of photoperiod on survival, growth, physiological, and biochemical indices of redclaw crayfish (*Cherax quadricarinatus*) juveniles. *Animals* **2024**, *14*, 411. [CrossRef]
6. Chen, S.; Liu, J.; Shi, C.; Migaud, H.; Ye, Y.; Song, C.; Mu, C.; Ren, Z.; Wang, C. Effect of photoperiod on growth, survival, and lipid metabolism of mud crab *Scylla paramamosain* juveniles. *Aquac. Res.* **2023**, *567*, e739279. [CrossRef]
7. Gao, X.; Pang, G.; Luo, X.; You, W.; Ke, C. Effects of light cycle on circadian feeding activity and digestive physiology in *Haliotis discus* hannai. *Aquac. Res.* **2021**, *539*, e736642. [CrossRef]
8. Imai, T.; Oonuki, T. Records of Chinese grass shrimp, *Palaemonetes sinensis* (Sollaud, 1911) from western Japan and simple differentiation method with native freshwater shrimp, *Palaemon paucidens* De Haan, 1844 using eye size and carapace color pattern. *BioInvasions Rec.* **2014**, *3*, 163–168. [CrossRef]
9. Zhao, Y.; Zhu, X.; Jiang, Y.; Li, Z.; Li, X.; Xu, W.; Wei, H.; Li, Y.; Li, X. Genetic diversity and variation of seven Chinese grass shrimp (*Palaemonetes sinensis*) populations based on the mitochondrial COI gene. *BMC Ecol. Evol.* **2021**, *21*, 167. [CrossRef]

10. Li, Y.; Liang, S.; She, Q.; Han, Z.; Li, Y.; Li, X. Influence of temperature and size on menthol anaesthesia in Chinese grass shrimp *Palaemonetes sinensis* (Sollaud, 1911). *Aquac. Res.* **2018**, *49*, 2091–2098. [CrossRef]
11. Li, Y.; She, Q.; Han, Z.; Sun, N.; Liu, X.; Li, X. Anaesthetic effects of eugenol on grass shrimp (*Palaemonetes sinensis*) of different sizes at different concentrations and temperatures. *Sci. Rep.* **2018**, *8*, 11007. [CrossRef] [PubMed]
12. Aoki, Y.; Sugimoto, Y.; Imai, T.; Tani, S.; Tettey, P.A.; Khalfan, A.-W.M.; Saito, H. Appearance of exotic shrimp *Palaemon sinensis* (Sollaud, 1911) and other freshwater shrimps before and after the 2018 extreme flood in western Japan. *BioInvasions Rec.* **2024**, *13*, 183–194. [CrossRef]
13. Han, Z.; Li, X.; Li, X.; Xu, W.; Li, Y. Circadian rhythms of melatonin in haemolymph and optic lobes of Chinese mitten crab (*Eriocheir sinensis*) and Chinese grass shrimp (*Palaemonetes sinensis*). *Biol. Rhythm Res.* **2019**, *50*, 400–407. [CrossRef]
14. Yingdong, L.; Huiling, X.; Xiaodong, L. Transcriptome analysis of the Chinese grass shrimp *Palaemonetes sinensis* (Sollaud 1911) and its predicted feeding habit. *J. Oceanol. Limnol.* **2018**, *36*, 1778–1787.
15. Changyue, Y.; Weibin, X.; Xin, L.; Jiaxin, J.; Xinmiao, Z.; Simiao, W.; Zhiyuan, Z.; Yanyu, W.; Qijun, C.; Yingdong, L. Comparative transcriptome analysis of Chinese grass shrimp (*Palaemonetes sinensis*) hepatopancreas under ectoparasitic isopod (*Tachaea chinensis*) infection. *Fish Shellfish Immunol.* **2021**, *117*, 211–219.
16. Mark, R.V. Metabolomics of aquatic organisms: The new 'omics' on the block. *Mar. Ecol. Prog. Ser.* **2007**, *332*, 301–306.
17. Hillyer, K.E.; Beale, D.J.; Shima, J.S. Artificial light at night interacts with predatory threat to alter reef fish metabolite profiles. *Sci. Total Environ.* **2021**, *769*, e144482. [CrossRef]
18. Yu, C.; Zhang, B.; Hu, N.; Li, L.; Wang, S.; Zhang, Z.; Wei, T.; Zhao, Y.; We, I.H.; Hu, Q.; et al. Comparative metabolomic analysis of Chinese mitten crab (*Eriocheir sinensis*) during the daily cycle. *Aquac. Res.* **2022**, *53*, 2947–2958. [CrossRef]
19. Zhou, X.; Li, Q.; Zhu, J.; Xie, S.; Wang, M.; Yang, T. Effects of hypoxic stress on tissue structure and gut bacterial community of *Exopalaemon carinicauda*. *Prog. Fish. Sci.* **2024**, *45*, 167–177.
20. Wang, L.; Xue, Y.; Jiang, G.; Shi, L.; Huang, X. *The Effects of Temperature and Feed on the Growth, Development, and Reproductive Performances of Neocaridina denticulata*; Shanghai Ocean University: Shanghai, China, 2024; pp. 1–22.
21. Thévenot, E.A.; Roux, A.; Xu, Y.; Ezan, E.; Junot, C. Analysis of the human adult urinary metabolome variations with age, body mass index, and gender by implementing a comprehensive workflow for univariate and OPLS statistical analyses. *J. Proteome Res.* **2015**, *14*, 3322–3335. [CrossRef] [PubMed]
22. Zhou, J.; He, W.-Y.; Wang, W.-N.; Yang, C.-W.; Wang, L.; Xin, Y.; Wu, J.; Cai, D.-x.; Liu, Y.; Wang, A.-L. Molecular cloning and characterization of an ATP-binding cassette (ABC) transmembrane transporter from the white shrimp *Litopenaeus vannamei*. *Comp. Biochem. Physiol. Part C Toxicol. Pharmacol.* **2009**, *150*, 450–458. [CrossRef] [PubMed]
23. Luo, S.-S.; Chen, X.-L.; Wang, A.-J.; Liu, Q.-Y.; Peng, M.; Yang, C.-L.; Yin, C.-C.; Zhu, W.-L.; Zeng, D.-G.; Zhang, B.; et al. Genome-wide analysis of ATP-binding cassette (ABC) transporter in *Penaeus vannamei* and identification of two ABC genes involved in immune defense against *Vibrio parahaemolyticus* by affecting NF-κB signaling pathway. *Int. J. Biol. Macromol.* **2024**, *262*, 129984. [CrossRef] [PubMed]
24. Seo, S.-K.; Kwon, B. Immune regulation through tryptophan metabolism. *Exp. Mol. Med.* **2023**, *55*, 1371–1379. [CrossRef] [PubMed]
25. Arumugham, V.B.; Baldari, C.T. cAMP: A multifaceted modulator of immune synapse assembly and T cell activation. *J. Leukoc. Biol.* **2017**, *101*, 1301–1316. [CrossRef]
26. Cameron, E.G.; Kapiloff, M.S. Intracellular compartmentation of cAMP promotes neuroprotection and regeneration of CNS neurons. *Neural Regener. Res.* **2017**, *12*, 201–202. [CrossRef]
27. Naderi, F.; Hernández-Pérez, J.; Chivite, M.; Soengas, J.L.; Míguez, J.M.; López-Patiño, M.A. Involvement of cortisol and sirtuin1 during the response to stress of hypothalamic circadian system and food intake-related peptides in rainbow trout, *Oncorhynchus mykiss*. *Chronobiol. Int.* **2018**, *35*, 1122–1141. [CrossRef]
28. Ren, X.; Zhang, J.; Wang, L.; Wang, Z.; Wang, Y. Diel variation in cortisol, glucose, lactic acid and antioxidant system of black sea bass *Centropristis striata* under natural photoperiod. *Chronobiol. Int.* **2020**, *37*, 176–188. [CrossRef]
29. Espinosa-Chaurand, D.; Vega-Villasante, F.; Carrillo-Farnés, O.; Nolasco-Soria, H. Effect of circadian rhythm, photoperiod, and molt cycle on digestive enzymatic activity of *Macrobrachium tenellum* juveniles. *Aquac. Res.* **2017**, *479*, 225–232. [CrossRef]
30. Wang, Y.; Yang, R.; Fu, Z.; Ma, Z.; Bai, Z. The photoperiod significantly influences the growth rate, digestive efficiency, immune response, and antioxidant activities in the juvenile scalloped spiny lobster (*Panulirus homarus*). *J. Mar. Sci. Eng.* **2024**, *12*, e389. [CrossRef]
31. Shiau, S.-Y.; Chin, Y.-H. Dietary biotin requirement for maximum growth of juvenile grass shrimp, *Penaeus monodon*. *J. Nutr.* **1998**, *128*, 2494–2497. [CrossRef] [PubMed]